

Fig. S1. Adherens and tight-junction markers demarcate a multicellular F-actin^{BELT} meshwork. (A) Schematic showing the localization of the cortical F-actin^{BELT} with respect to apical-surface (Muc1), tight junction (ZO1), and adherens-junction (Ecad). (B-D) Representative *en face* images of Ecad and ZO1 in relation to the F-actin^{BELT} network. (E-H') Confocal steps (z-direction, 1.0 μm/step) through a plane of representative epithelial cells. Note the progression from Ecad (blue) through to intense F-actin signal and ZO1. Scale Bars in *B*, *C*, & *D* are 10 μm, and 5 μm in *E-H'*.

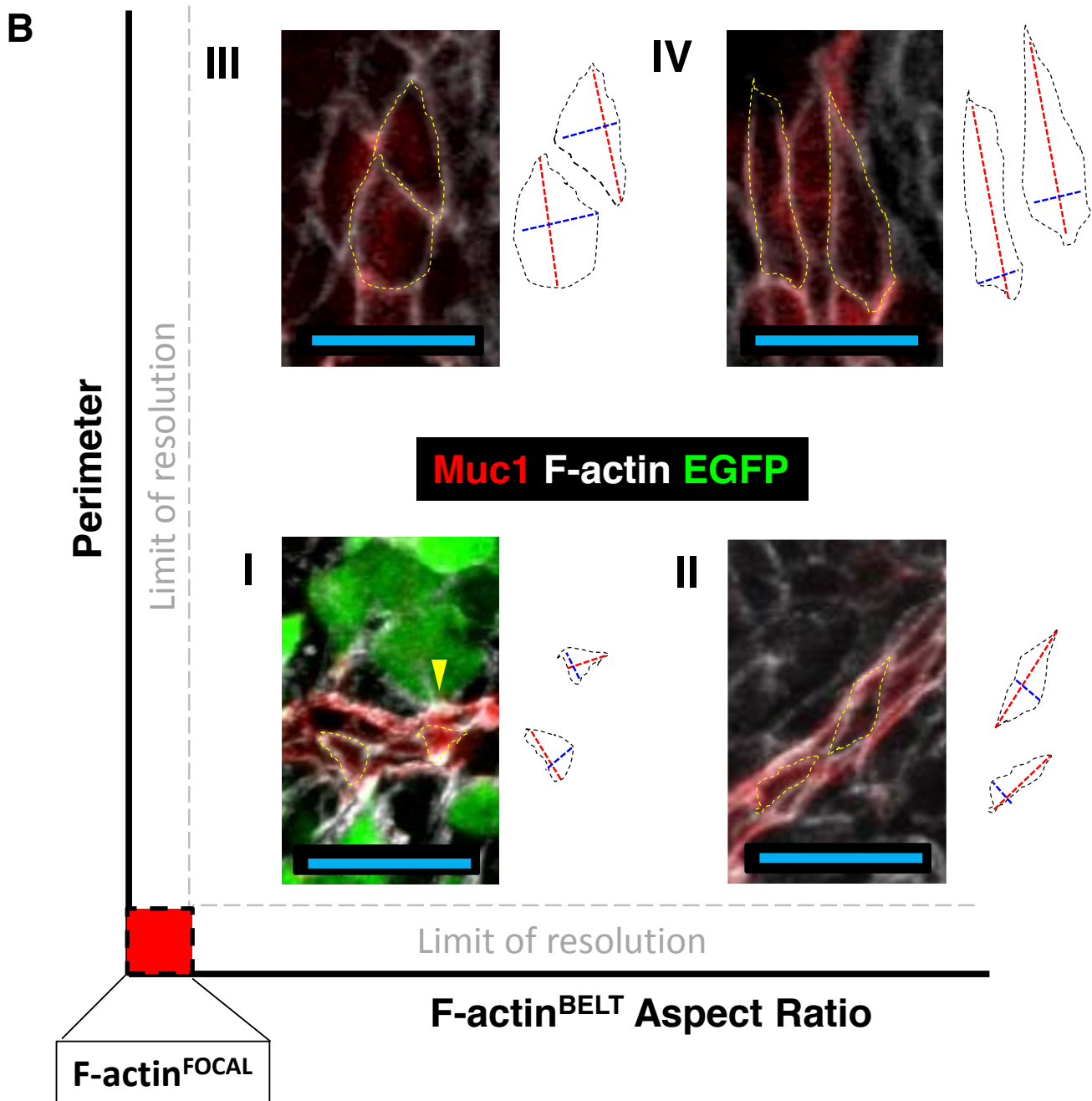
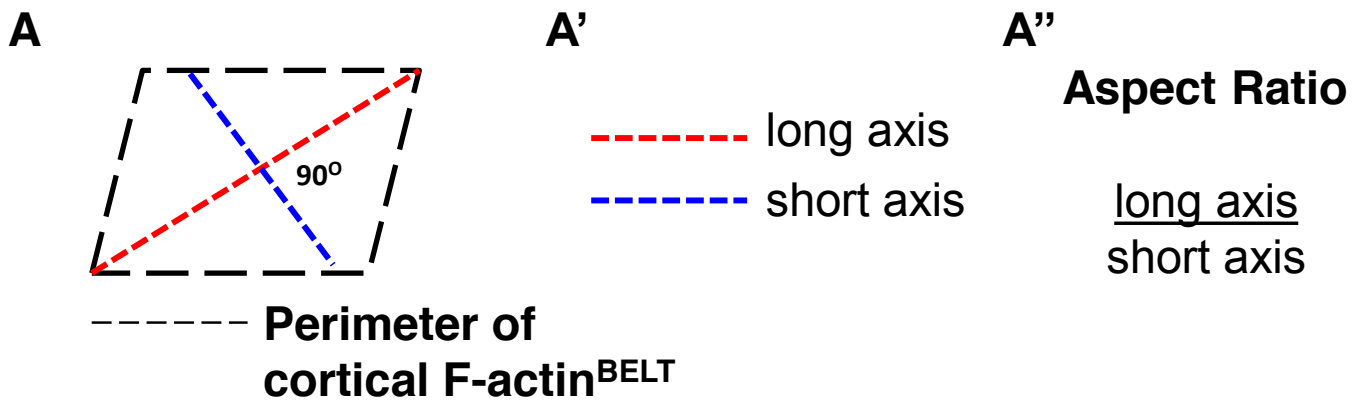


Fig. S2. F-actin^{BELT} aspect ratio versus perimeter defines the spectrum of F-actin^{BELT} sizes in epithelial populations. (A) Schematic of a typical cortical F-actin^{BELT} near apical surface an epithelial cell. Perimeter (black line) demarcates the F-actin^{BELT}. (A') Long axis (red dashed line) and short axis (blue dashed line set perpendicular (90°) to the pre-set long axis) defines axial dimensions of the F-actin^{BELT}. (A'') Aspect ratio is defined by the divisional product of the long and short axis. (B) Schematic with examples of typical extremes in observed F-actin^{BELT} dimensions (F-actin^{BELT} traced in yellow dashed line). Roman numeral I indicates narrowed apical cortex. Roman numeral II indicates elongated F-actin^{BELT}. Roman numeral III indicates expanded F-actin^{BELT}. Roman numeral IV indicates expanded and elongated F-actin^{BELT}. Grey dashed line demarcates limit of resolution in x and y for accurate measurement by our methods (~2.0 μm). F-actin^{FOCAL} perimeter and aspect ratio are below minimum resolution or at the origin (red box). Yellow arrowhead marks typical F-actin^{FOCAL} structure at the apical surface of an egressing Neurog3^{EGFP/+} reporting⁺ cell. Scale bars are 20 μm.

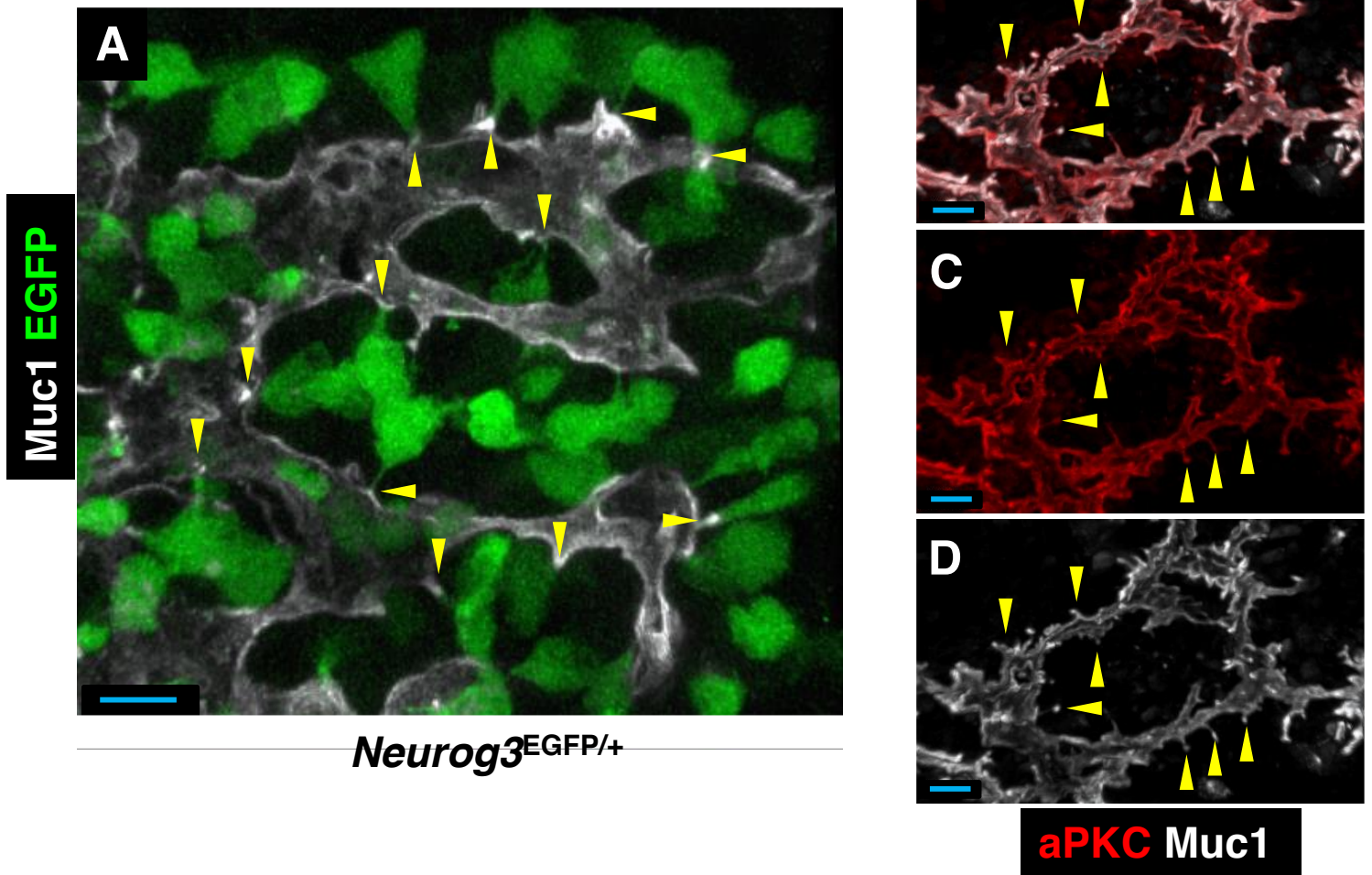


Fig. S3. Epithelially egressing endocrine cells maintain a narrow apical lumen-surface contact. (A) Representative 40x confocal z-stack of E14.5 *Ngn3*^{EGFP/+} plexus showing apical lumen-surface contact of delaminating EGFP-reporting cells. (B-D) Immunodetection of aPKC and Muc1 showing their localization at representative Muc1⁺ F-actin^{FOCAL} structures (yellow arrowheads). Scale bars are 10 μm in A-D.

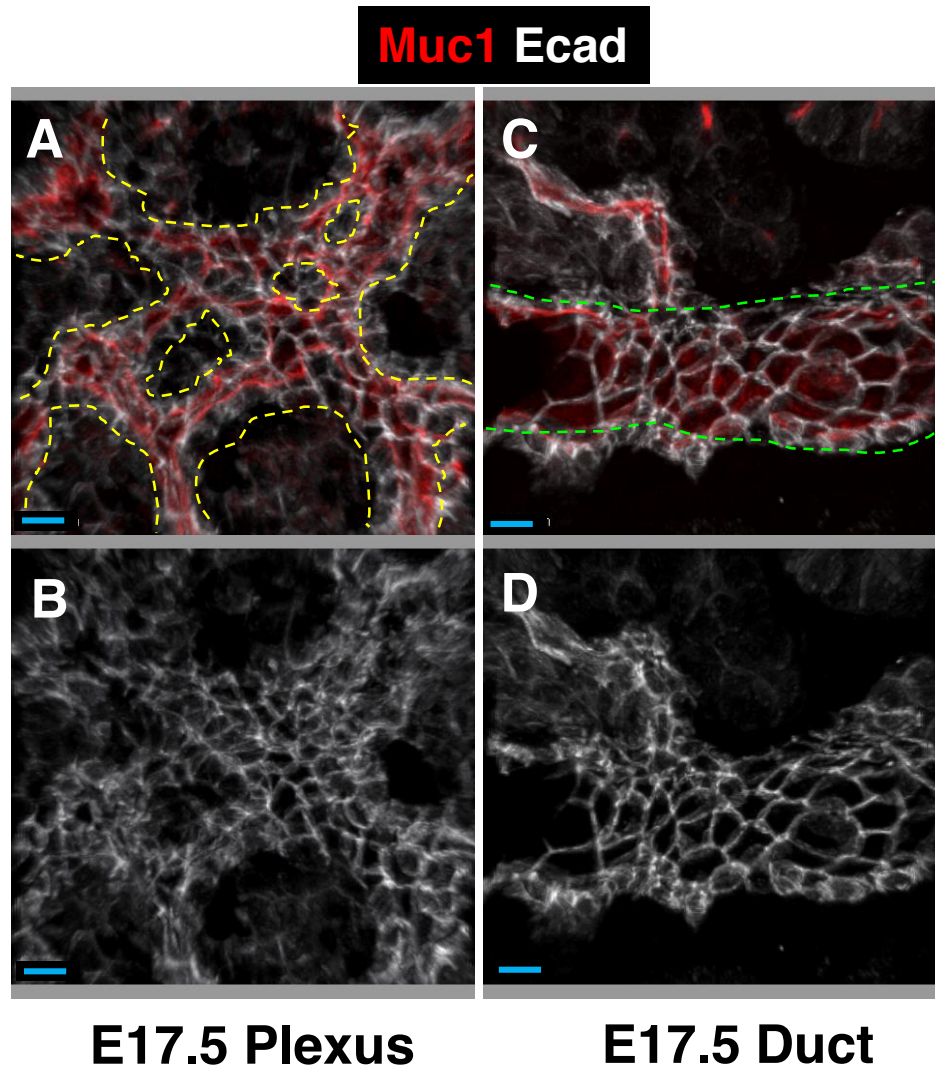


Fig. S4. E-cadherin immunolabeling shows enlargements in cell shape in the duct-state compared to the plexus. (A,B) Confocal z-stack of Muc1 and Ecad markers showing cell morphologies in the plexus at E17.5 (plexus traced by yellow dashed line). (C,D) Confocal z-stack of cell dimensions and shapes in the duct at E17.5 (duct traced by green dashed line). Scale bars are 10 μm .

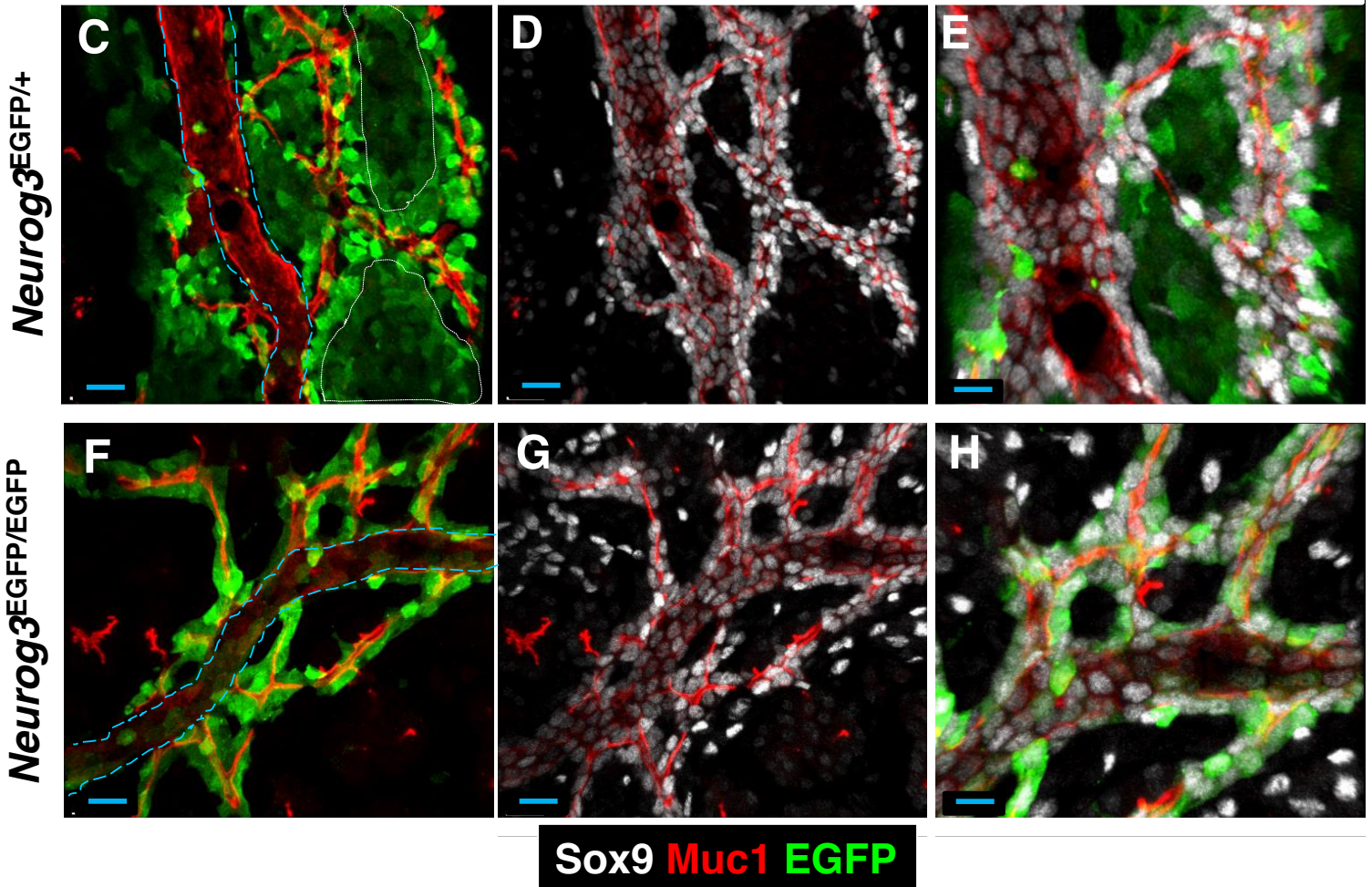
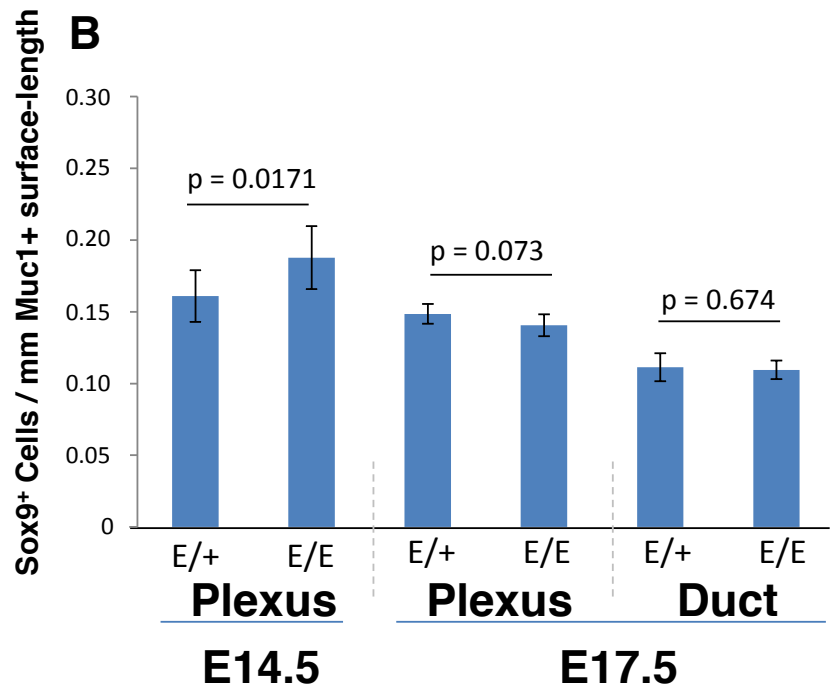
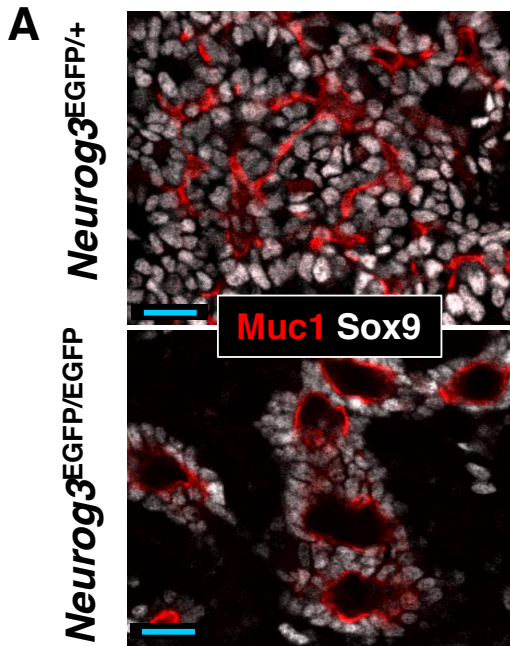


Fig. S5. Increased Sox9⁺ cell packing in the *Neurog3*-null epithelium is corrected by late gestation. (A,B) Measurements on the number of Sox9⁺ nuclei along the length of Muc1⁺ lumen *Neurog3*^{EGFP/+} versus *Neurog3*^{EGFP/EGFP} epithelium at E14.5 and E17.5, respectively. (C-H) Representative thick sections of Muc1, Sox9 and EGFP in duct and plexus states at E17.5. Cyan dashed lines in C and F demarcate the duct from the plexus-state, and white trace marks low EGFP expression in the forming endocrine islets. Scale bars are 20 μm in C,D,F,G; 10 μm in E,H.

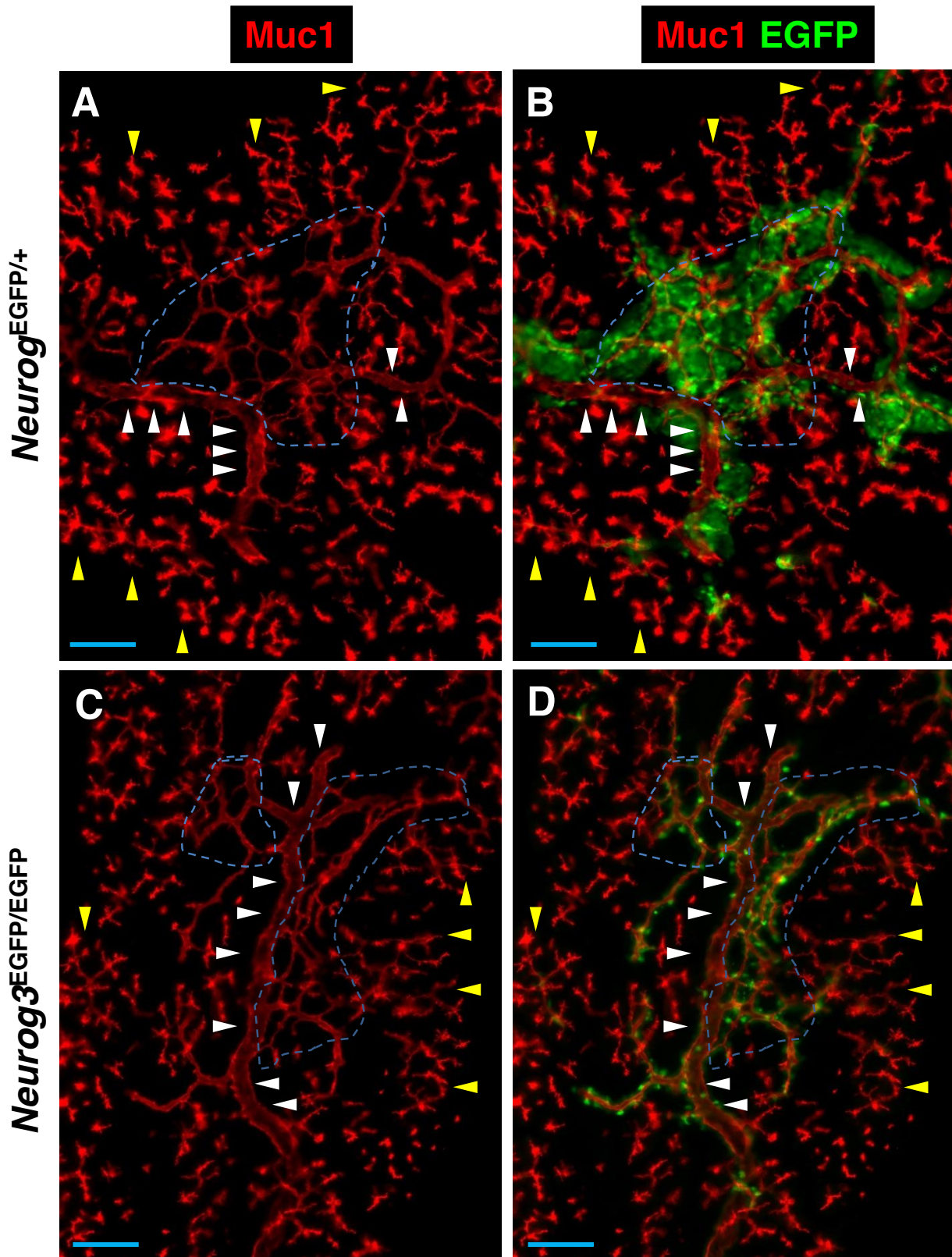


Fig. S6. *Neurog3* is broadly upregulated in cells within the plexus at late gestation. (A-D) Wide-field 10x epifluorescence images of thick-sectioned pancreas (30 μ m) showing *Neurog3*-expressing cells in the plexus (blue dashed line), duct (white arrowheads), and peripheral ductal branches (yellow arrowheads) in *Neurog3*^{EGFP/+} and *Neurog3*^{EGFP/EGFP} epithelium at E18.5. Scale bars are 100 μ m.

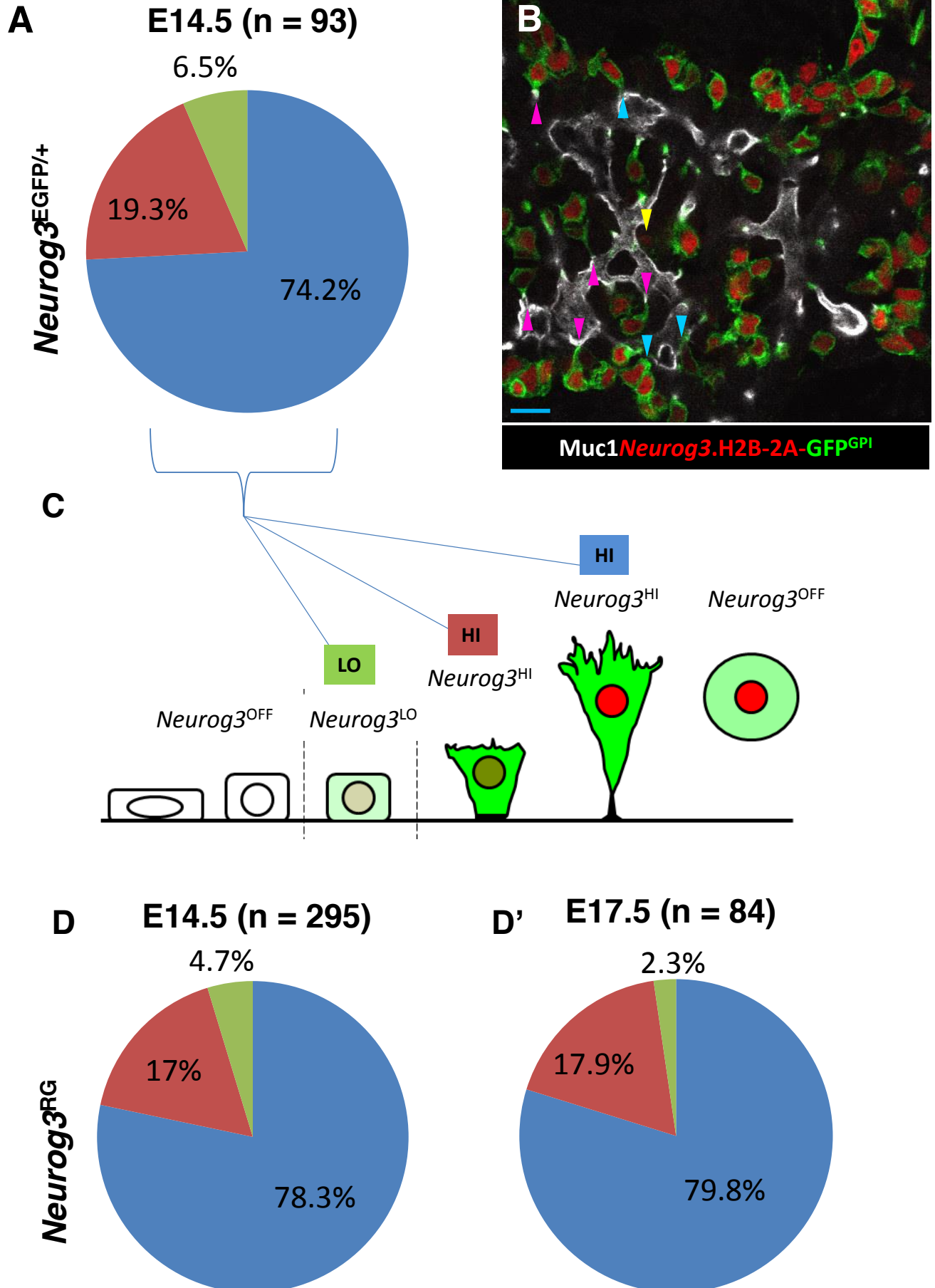


Fig. S7. Quantification of *Neurog3*-expressing states using *Neurog3* knock-in and BAC-transgenic reporter alleles. (A) Quantification of the proportions of non-apically narrowed (green), apically narrowed (red), and focalized and basally displaced (blue) *Neurog3*^{EGFP/+} cells at E14.5. (B) *Neurog3*^{RG+} cells in a representative z-stack labeled with Muc1 at E14.5. Yellow arrowhead marks non-apically narrowed *Neurog3*^{RG-LO} cell, cyan arrowheads mark apically narrowed *Neurog3*^{RG-HI} cells, pink arrowheads mark *Neurog3*^{RG-HI} cells associated with F-actin^{FOCAL} structures. Scale bar is 20 μ m. (C,C') Diagram of the principal cell-morphological states associated with *Neurog3*^{OFF}, *Neurog3*^{LO}, and *Neurog3*^{HI} populations, color coded to match A-B. (D,D') Percentage of non-apically narrowed (green), apically narrowed (red), and focalized and basally displaced (blue) *Neurog3*^{RG+} cells at E14.5 and E17.5.

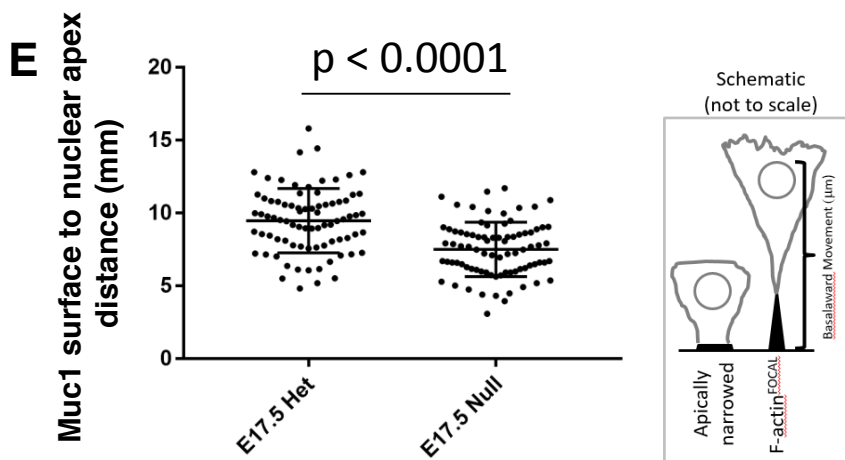
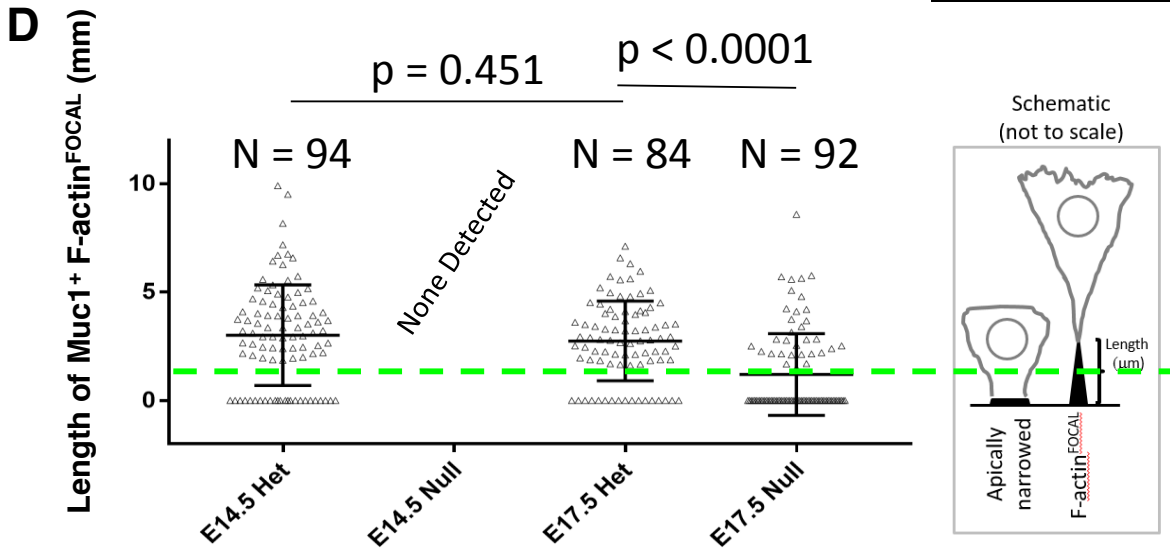
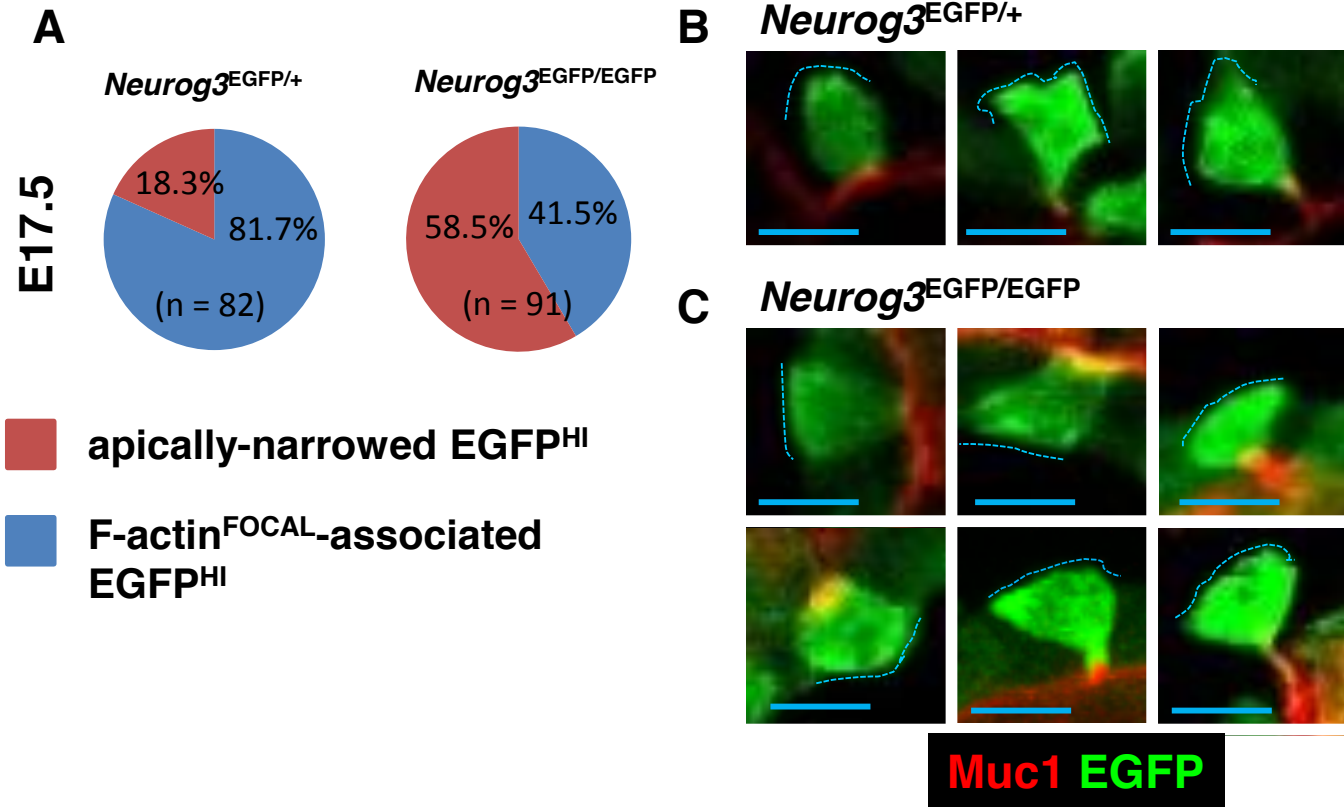


Fig. S8. *Neurog3*-deficient *Neurog3*^{HI} cells show defective apical narrowing, F-actin^{FOCAL} formation, and basalward cell movement. (A) Proportion of EGFP^{HI} cells that exhibit a narrowed apical surface versus a fully formed F-actin^{FOCAL} structure in *Neurog3*^{EGFP/+} and *Neurog3*^{EGFP/+} plexus at E17.5. (B) Images of EGFP^{HI} cells in *Neurog3*^{EGFP/+} pancreata undergoing *Neurog3* upregulation during apical narrowing and F-actin^{FOCAL} formation. Note the migratory protrusions at the basal cell surface (dashed cyan lines). (C) Images of EGFP^{HI} cells in *Neurog3*^{EGFP/EGFP} pancreata undergoing *Neurog3* upregulation during apical narrowing and F-actin^{FOCAL}-formation. (D) Measurements of the lengths of typical F-actin^{FOCAL} structures associated with EGFP^{HI} cells in *Neurog3*^{EGFP/+} and *Neurog3*^{EGFP/EGFP} epithelium at E14.5 and E17.5. Green dashed line indicates the distinction between an apically-narrowed surface (below line; beyond limit of accurate measure) versus a fully formed F-actin^{FOCAL} structure (above line). (E) Measurement of basalward movement was determined as the distance from the Muc1⁺ lumen surface to the basal-most aspect of the nucleus of EGFP^{HI} cells in *Neurog3*^{EGFP/+} and *Neurog3*^{EGFP/EGFP} epithelium at E17.5. Scale bars are 7 μ m in B,C.

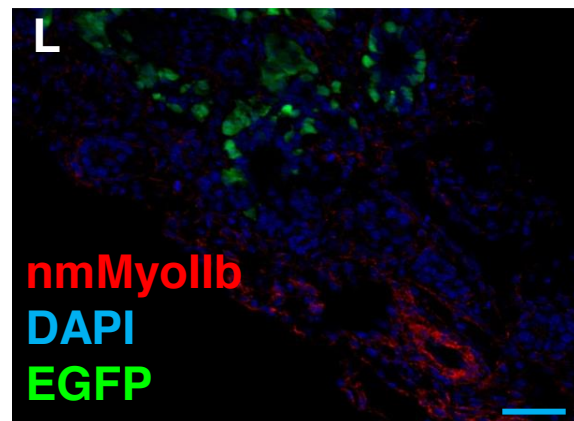
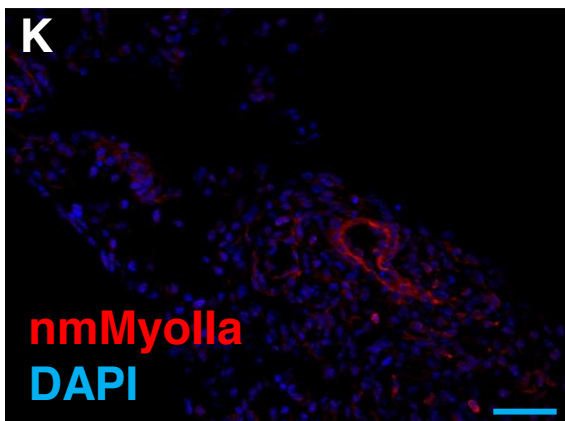
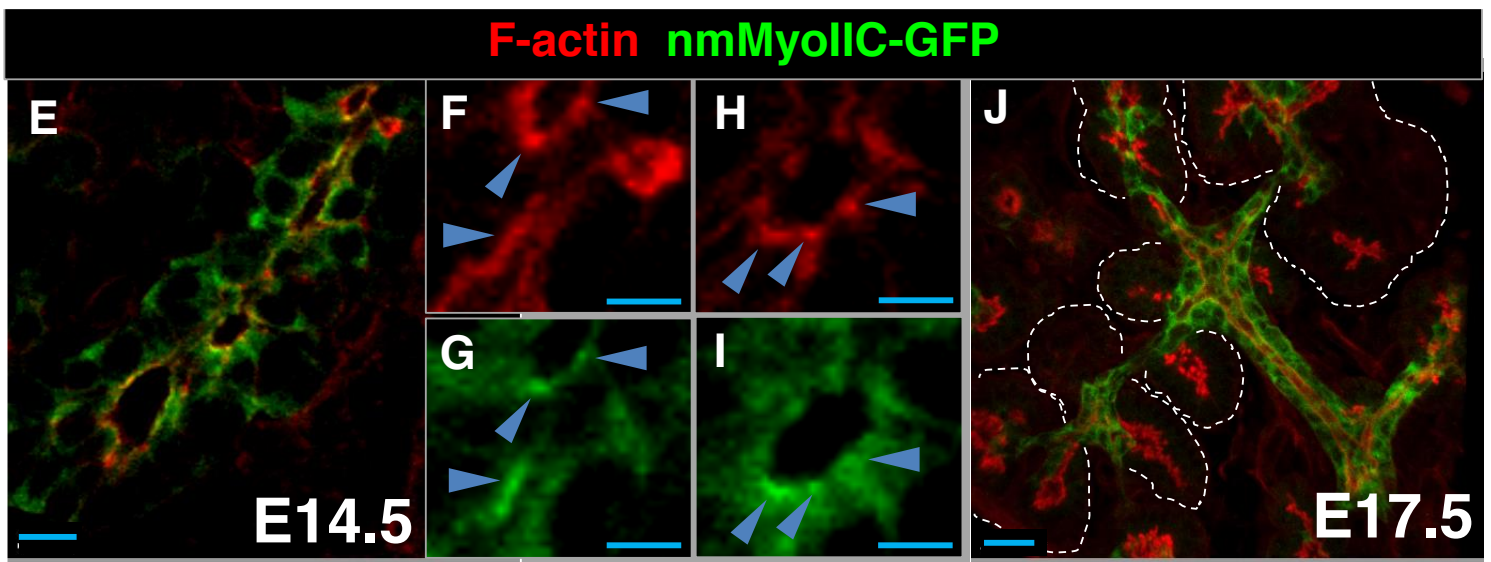
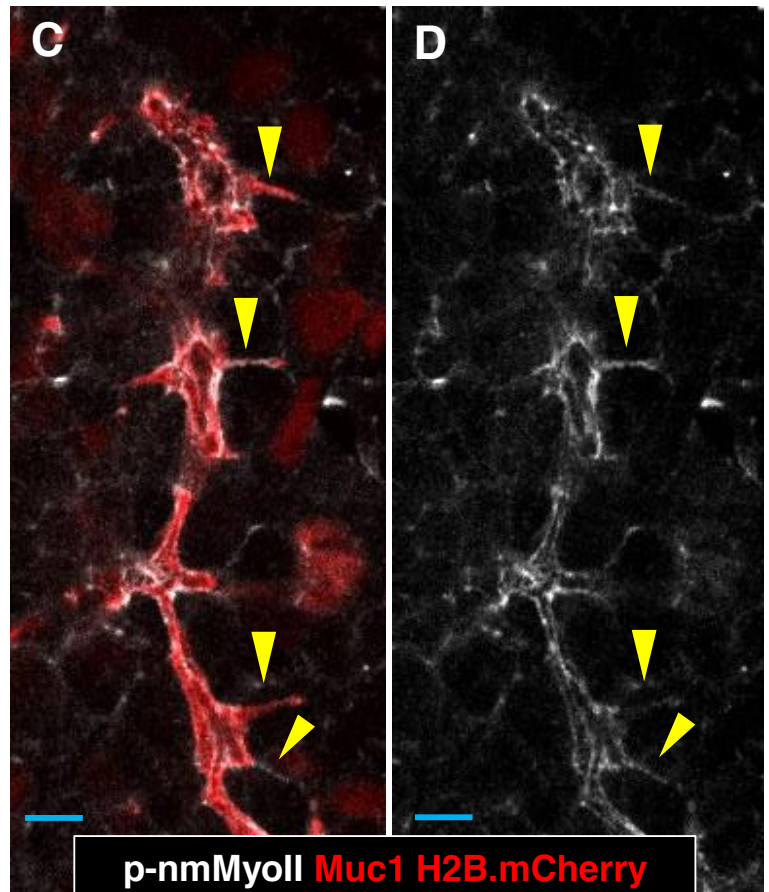
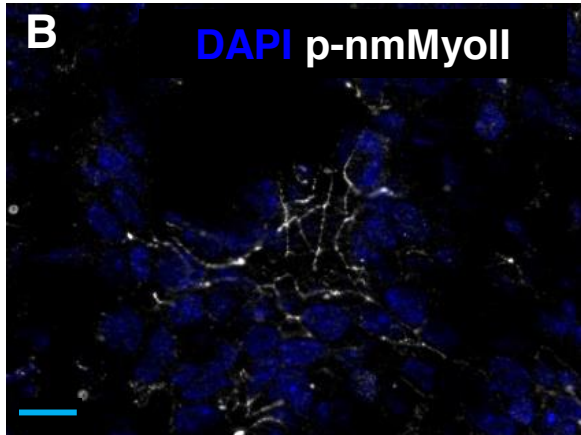
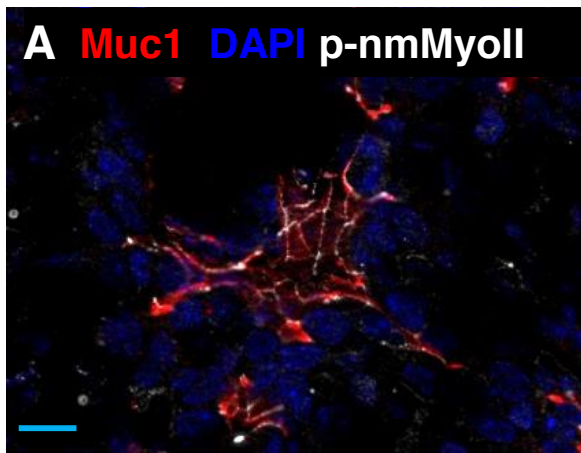
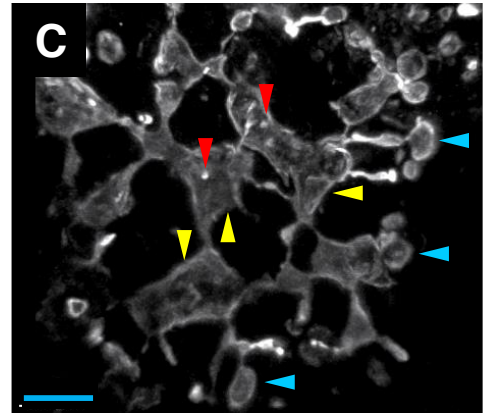
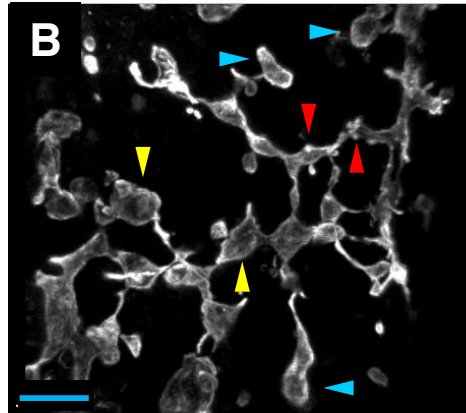
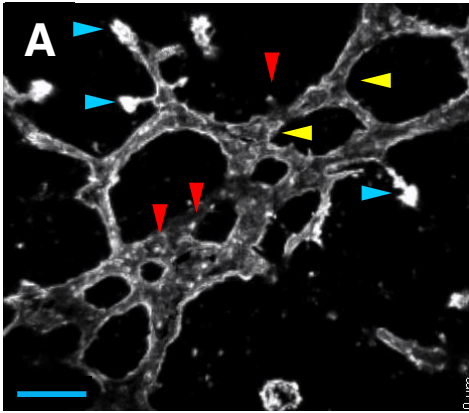


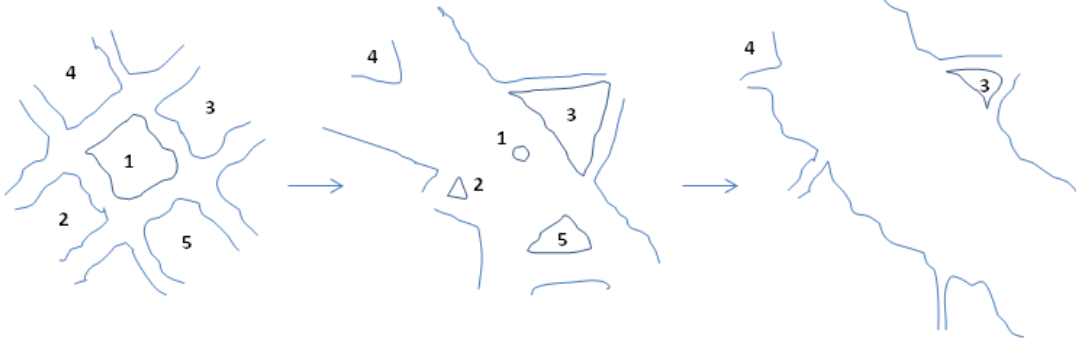
Fig. S9. nmMyoII isoforms are expressed and activated in the embryonic pancreas. (A,B) Separated fluorescence channels of p-nmMyoII along the Muc1⁺ lumen surface at E14.5. (C,D) P-nmMyoII localization along F-actin^{FOCAL} structures (yellow arrowheads) in the *Neurog3*^{RG} mouse strain. Muc1 and nuclear H2B-mCherry are shown in red, to indicate the lumen surface of *Neurog3*-expressing cells. (E) Localization of nmMyoIIC-GFP fusion protein in epithelial cells at E14.5. (F-I) Elevated nmMyoIIC-GFP signal is associated with intense phalloidin signal near the apical surface. (J) NmMyoIIC-GFP signal becomes enriched in the non-acinar epithelium by E17.5 (white dashed line demarcates acinar clusters). (K,L) nmMyoIIa and nmMyoIIb isoforms detected in the parenchyma (main blood vessels and mesenchyme) of the embryonic pancreas. EGFP signal is from the *Neurog3*^{EGFP/+} knock-in mouse strain. Scale bars are 10 μ m in A,B,E, 5 μ m in C,D,F-I, 20 μ m in J, and 100 μ m in K,L.

DMSO

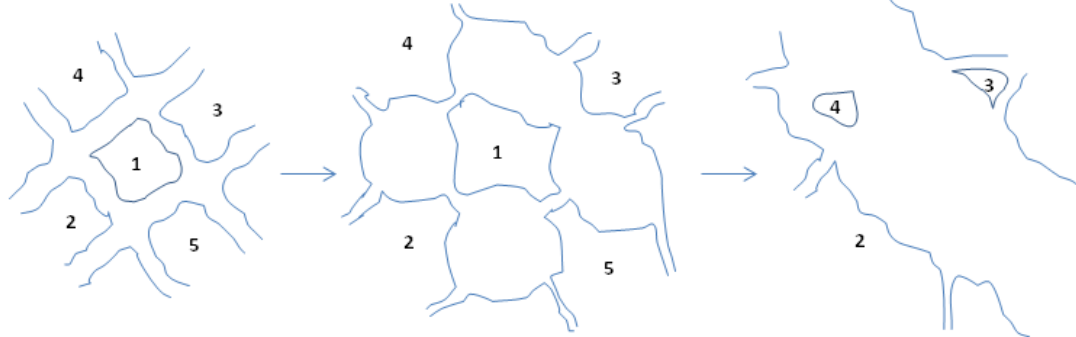
50 μ M BBS



D Plexus-to-duct transformation *in vivo* (~ 2 days, E15.5-E17.5)



E Plexus-to-duct-like transformation *ex vivo* (E15.5 + 18 hrs)



F

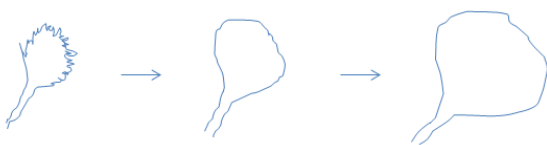
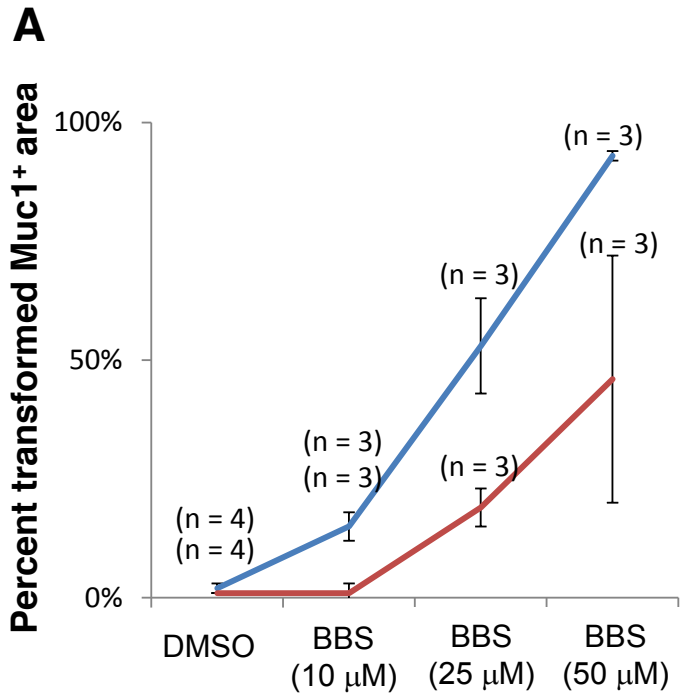
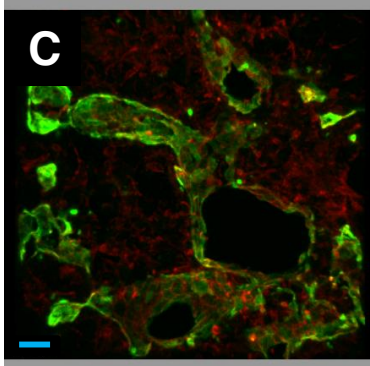
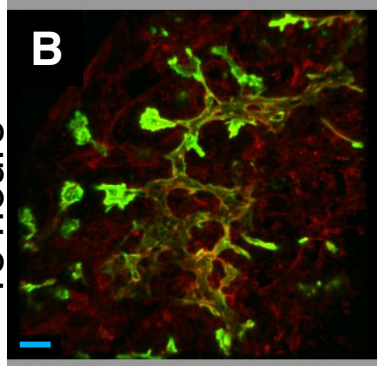


Fig. S10. NmMyoII-inhibition causes an abnormal plexus to duct-like transformation. (A) Qualities of the normal plexus state in vehicle-treated explants. (B-C) Representative images of abnormal plexus observed in BBS-treated explants. Qualities of the abnormal plexus state include localized bulb-like dilations of the epithelium (yellow arrowheads), malformed terminal acinar lumens (cyan arrowheads), and diminished numbers of F-actin^{FOCAL} structures (red arrowheads). Scale bars are 20 μ m. (D) Proposed diagram depicting typical plexus-to-duct transformations observed under normal (*in vivo*) and (E) nmMyoII-inhibited conditions. Note the difference in time scales. (F) Depiction of the process of acinar lumen dilation observed under nmMyoII-inhibited conditions.



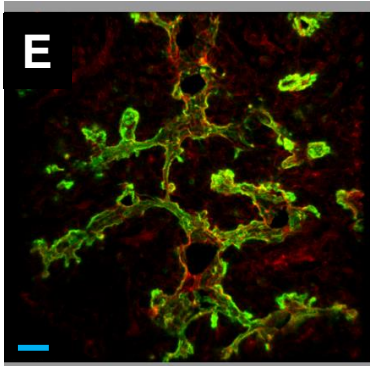
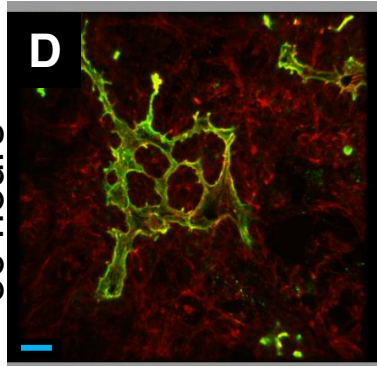
DMSO

25 μM BBS



DMSO

Washout



Muc1 F-actin

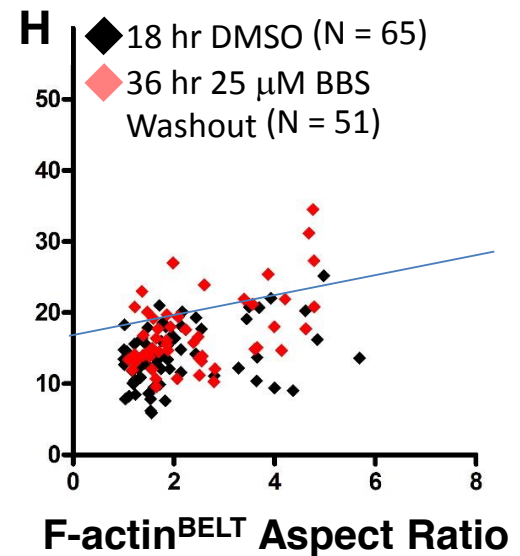
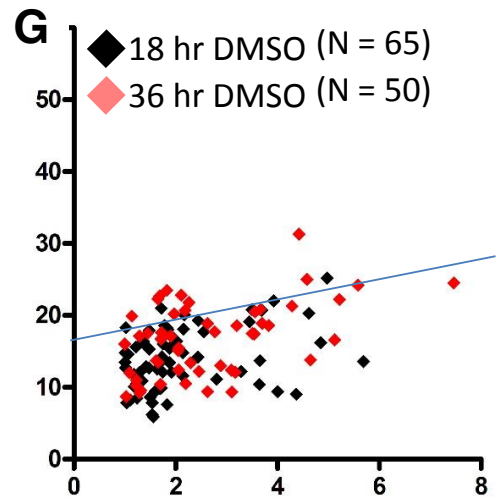
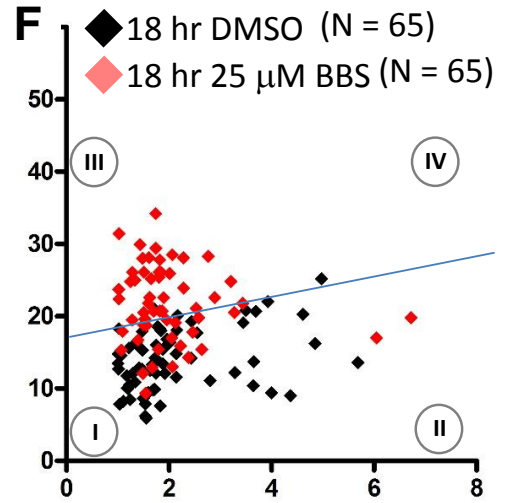


Fig. S11. Effects of BBS treatment on the plexus are dose-dependent and reversible. (A) Measurements of the relative Muc1⁺ pixel area exhibiting full duct-like transformation (red line), or abnormal plexus-state morphology (blue line), in explants grown in increasing concentrations of BBS for 18 hrs. Muc1 and F-actin localization in explants grown for 18 hr in DMSO (B), 18 hrs in 25 μ M BBS (C), 36 hrs in DMSO (D), or 18 hrs in 25 μ M BBS with a subsequent washout and 18 hr culture in DMSO (D). (F) Dimensions of F-actin^{BELT} in plexus treated with DMSO for 18 hrs (black dots *F,G,H*) or 25 μ M BBS for 18 hrs (red dots) used as reference for *G,H*. (G) Dimensions of F-actin^{BELT} in plexus treated with DMSO for 36 hrs (red dots). (H) Dimensions of F-actin^{BELT} in plexus treated with 25 μ M BBS for 18 hrs, with a subsequent washout and 18 hr culture in DMSO (red dots). Blue line indicates the maximum on the y-axis for F-actin^{BELT} dimensions measured in the plexus *in vivo*. Scale bars are 20 μ m.

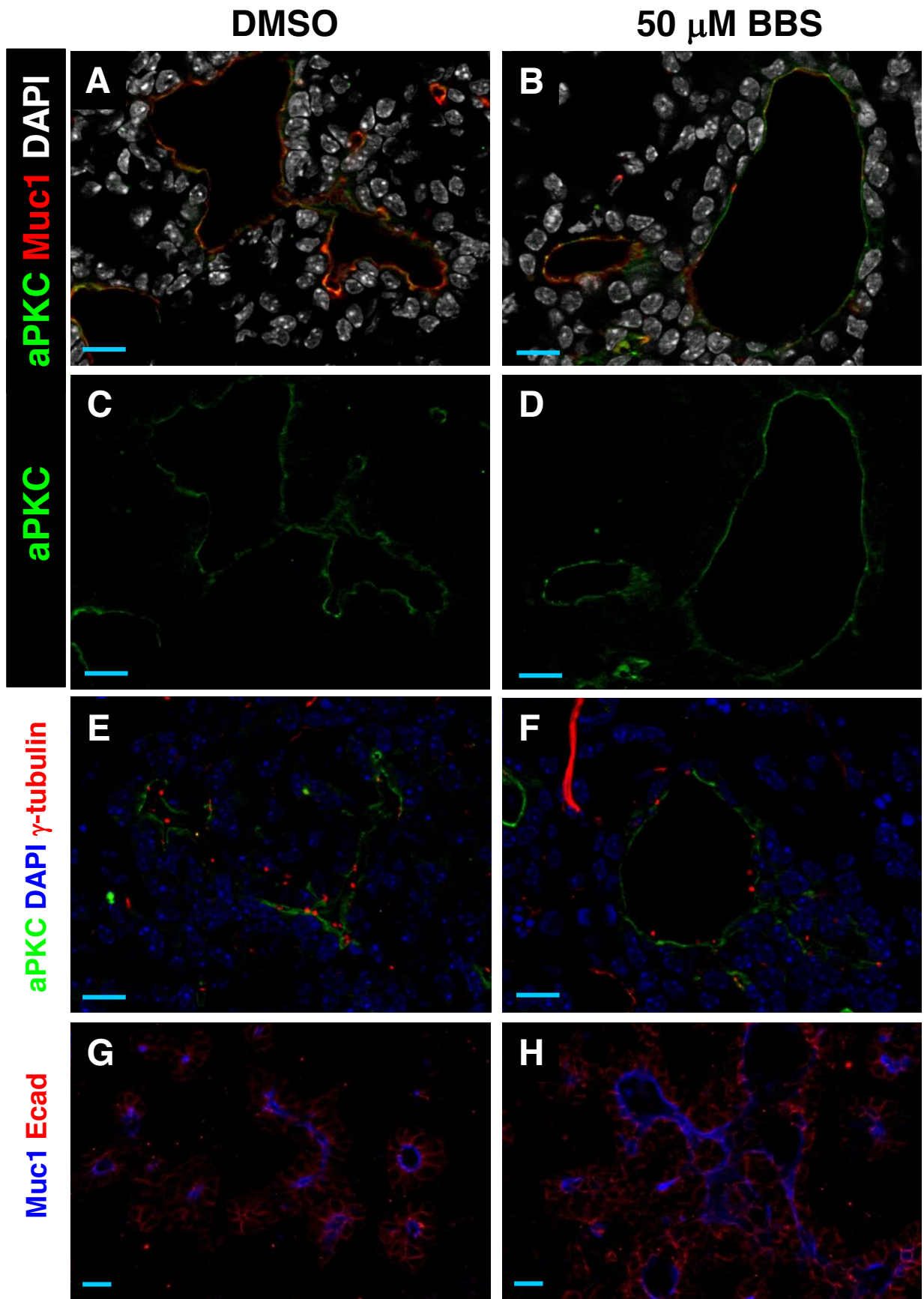


Fig. S12. Apical polarity and cell contact is maintained under nmMyoII-inhibited conditions. (A-D) Representative images of E14.5 plexus explants treated for 18 hr with DMSO or 50 μ M BBS and labeled with the apical markers Muc1, and aPKC. (E,F) Untreated and treated samples labeled with the ciliary basal-body marker gamma-tubulin, which is normally localized near the aPKC⁺ apical surface of epithelial cells. (G,H) E-cadherin localization in epithelial cells from treated and untreated explants. Scale bars are 10 μ m.

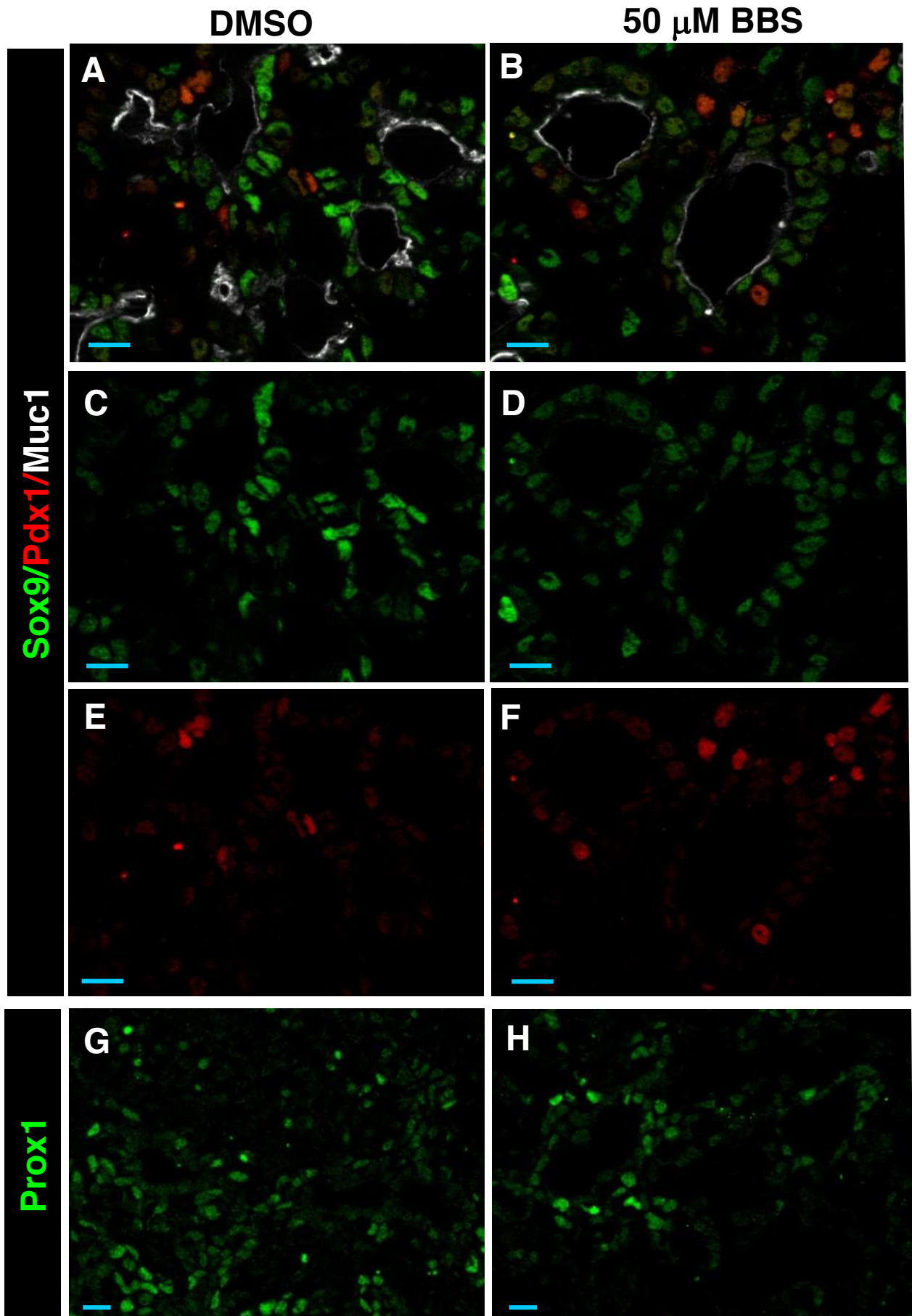
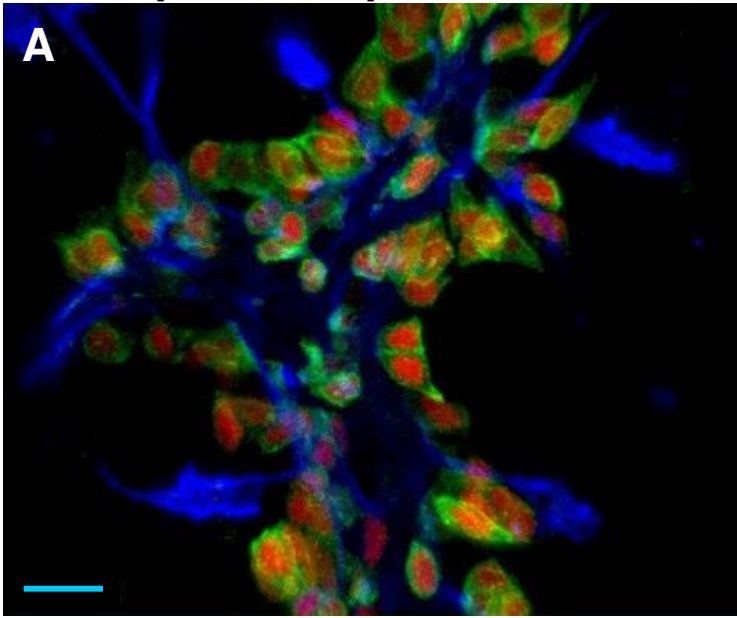
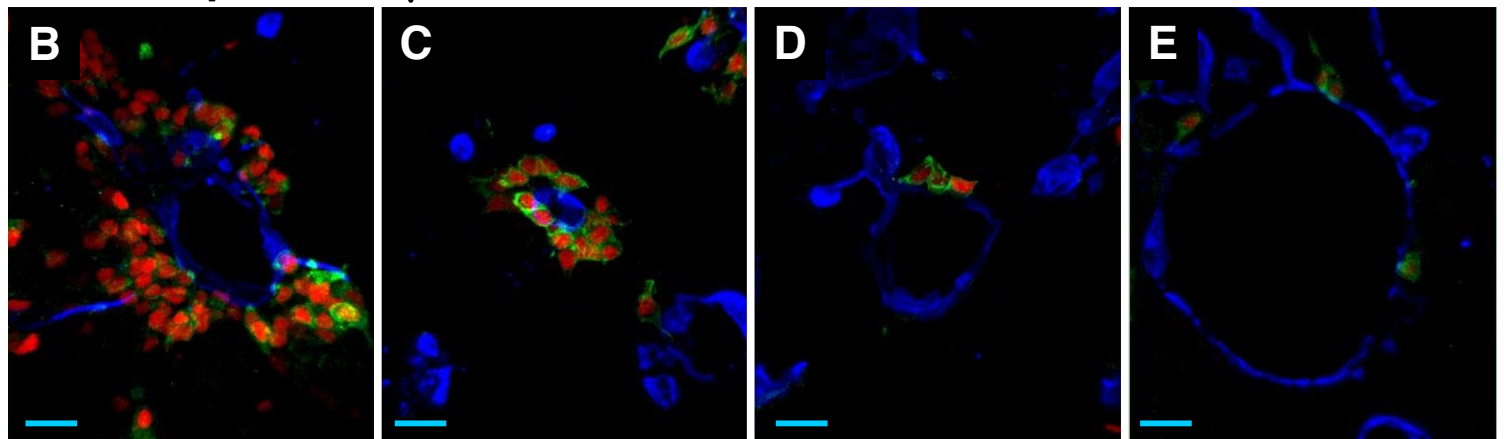


Fig. S13. Selective alterations in epithelial transcription-factor levels under nmMyoII-inhibited conditions. (A-F) Immunodetection of Sox9 and Pdx1 in plexus explants treated with DMSO or 50 μ M BBS for 18 hrs. (G,H) Expression of Prox1 in plexus explants treated with DMSO or 50 μ M BBS for 18 hrs. Scale bars are 10 μ m.

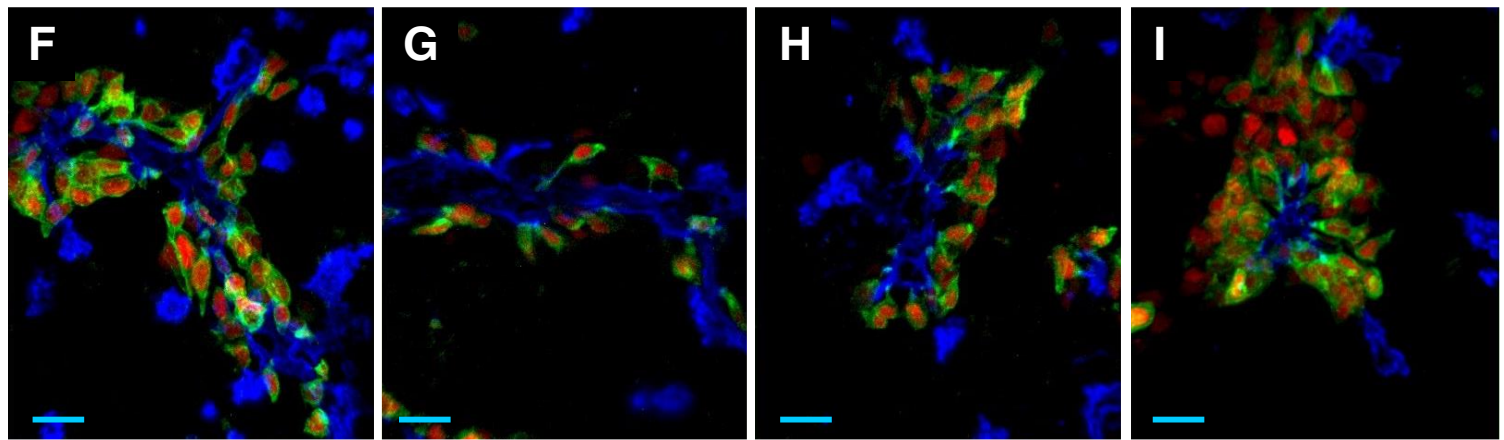
E15.5 plexus explant, DMSO-treated



E15.5 explant, 25 μ M BBS



E15.5 explant, 10 μ M Y27632



Muc1 mCherry GFP-GPI

Fig. S14. ROCK-nmMyoII pathway inhibitors influence luminal expansion, apical narrowing, and basalward migratory processes during *Neurog3* activation and upregulation. (A) Muc1⁺ lumen morphology and *Neurog3*^{RG+} cell morphology in untreated, BBS-treated (B-E), and Y27632-treated (F-I) explants. Scale bars are 15 μ m.

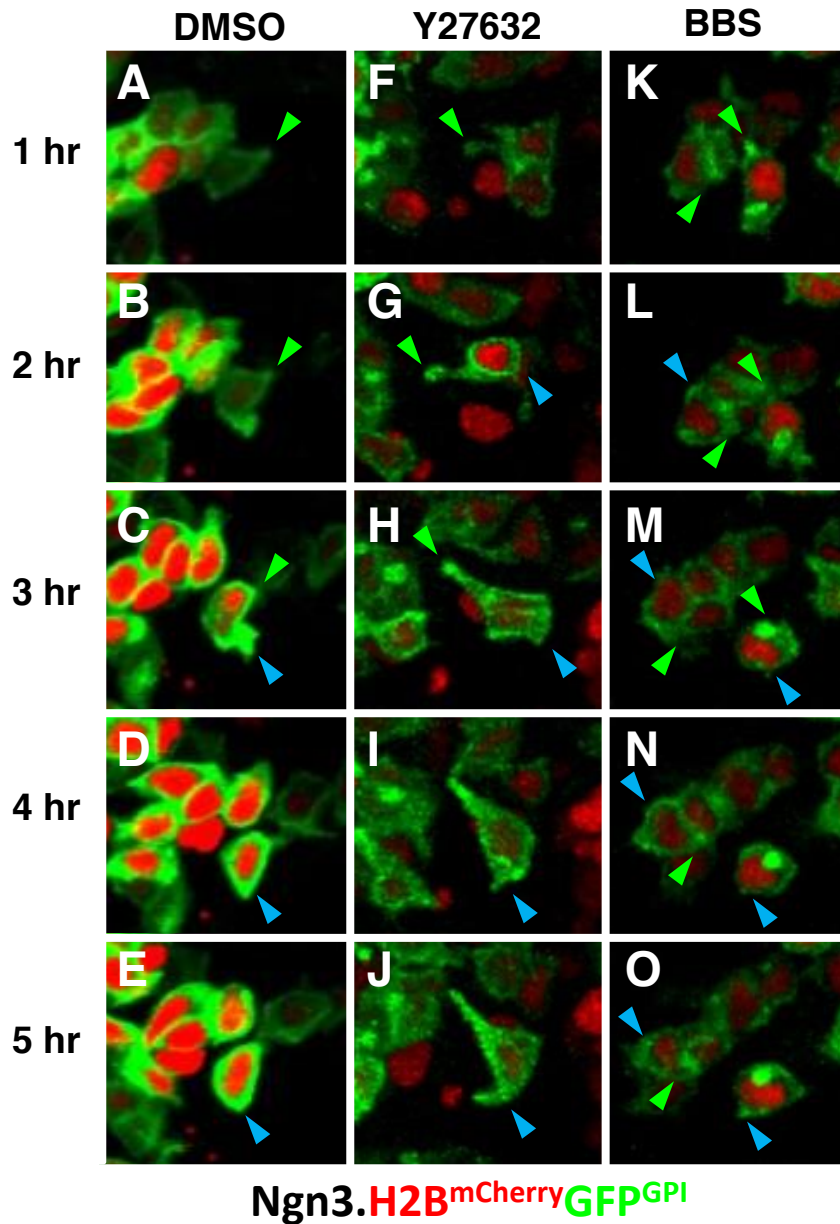


Fig. S15. Still frames from live imaging of endocrine-cell birth under nmMyoII- and ROCK-inhibited conditions. Still frames taken from time-lapse imaging experiments of *Neurog3^{RG+}* cells cultured in vehicle alone (A-E), Y27632 (F-J), or BBS (K-O). Snapshots were extracted at one-hour intervals marked after commencement of imaging, which begins between 1-2 hours after drug administration. N = 1 for each condition. Green arrowheads mark the apical aspect of the *Neurog3^{RG+}* cell. Blue arrowhead marks the basal surface of *Neurog3^{RG+}* cells.

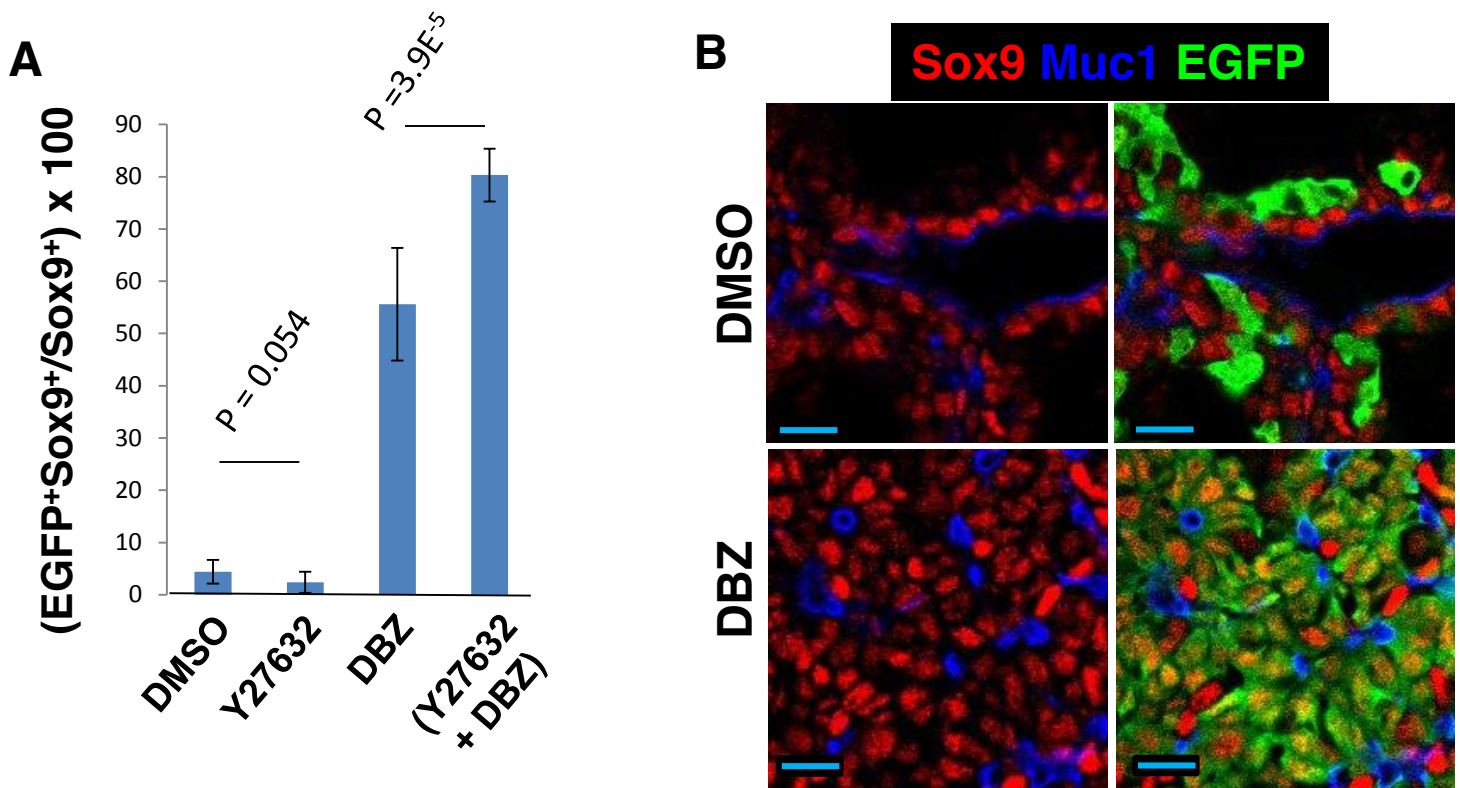


Fig. S16. ROCK and Notch inhibit *Neurog3* upregulation through distinct mechanisms. (A) Quantification of the proportion of Sox9⁺ epithelial cells that upregulate *Neurog3* in response to ROCK inhibition, Notch inhibition, or both in combination, in *Neurog3*^{EGFP/+} explants. Note that ROCK inhibition has little to no effect in promoting *Neurog3* upregulation unless Notch signaling is inhibited. (B) Images of Sox9 and EGFP in DMSO and DBZ-treated *Neurog3*^{EGFP/+} explants. Note the large number of Sox9⁺ and EGFP⁺ cells in the DBZ treated condition, which are only rarely observed in control tissue. Scale bars are 10 μ m.

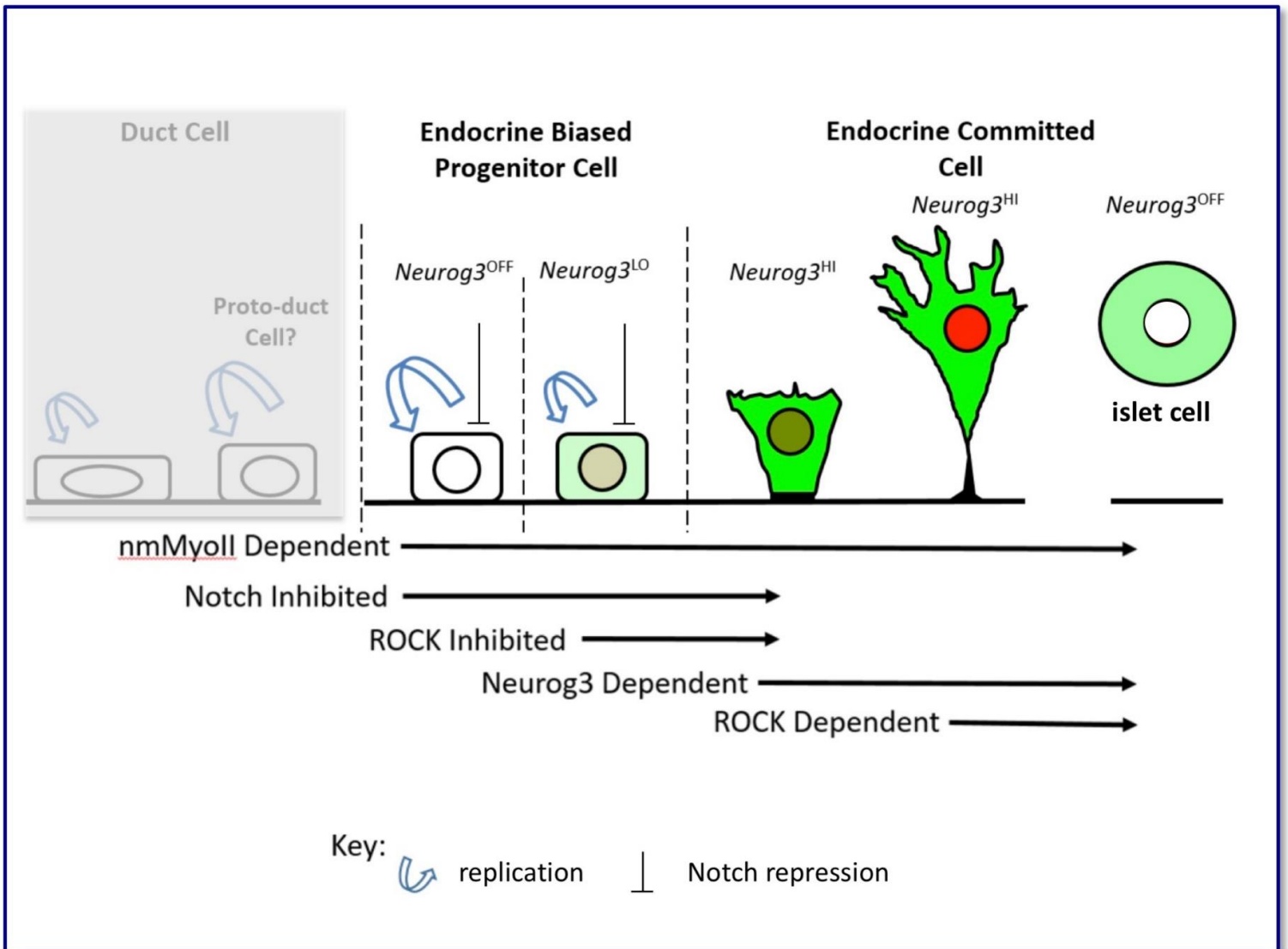


Fig. S17. Schematic of sequential steps in endocrine cell birth regulated by ROCK-nmMyoII, Notch, and Neurog3.

Table S1. Genotyping primers

<i>Neurog3</i> ^{EGFP}		
Ngn3-1		
Ngn3-2	5'-ATACTCTGGTCCCCCGTG-3'	Lee et al., 2002
EGFP	5'-TGTTTGCTGAGTGCCAATC-3'	Lee et al., 2002
<i>Neurog3</i> ^{FLOX}		
	5'-GAACTTGTGGCCGTTTACGT-3'	Lee et al., 2002
722	5'-CTATCCACTGCTGCTTGTCCTG-3'	Wang et al., 2008
723	5'-TGTGTCTCTGGGGACACTTGGAT-3'	Wang et al., 2008
Jv45	5'-TTCCGGTTATTCAACTTGCACC-3'	Wang et al., 2008

Table S2. Antibodies

<i>Antigen</i>	<i>Source</i>	<i>Dilution</i>	<i>Method</i>	<i>Company</i>
Muc1	Hamster	1:1000	Indirect IF	NeoMarkers
Sox9	Rabbit	1:5000	Indirect IF	Millipore
Neurog3	Goat	1:40,000	Biotin amplification	G. Gu (Vanderbilt)
EdU				Molec. Probes
Pdx1	G. Pig	1:1000	Indirect IF	C. Wright (Vanderbilt)
Ecad	Rat	1:2000	Indirect IF	AbCam
EGFP	Chick	1:2000	Indirect IF	Aves
DAPI			Mounting Medium	Life Tech.
Phalloidin		1:400	Direct Label	Molecular Probes
ZO-1	Rabbit	1:100	Indirect IF	Invitrogen
aPKC	Rabbit	1:400	Indirect IF	Santa Cruz
p-nmMyoII	Rabbit	1:200	Biotin Amplification	AbCam
nmMyoIIA	Rabbit	1:500	Indirect IF	Biolegend
nmMyoIIB	Rabbit	1:500	Indirect IF	Cell Signaling
γ -tubulin	Rabbit	1:1000	Biotin Amplification	AbCam
Prox1	Rabbit	1:1000	Indirect IF	AngioBio